Electronic Supplementary Material (ESI) for ChemComm.

Supporting information

Mechanism investigation of enhanced oxygen storage performance of $YBaCo_4O_{7+\delta}$ synthesized by glycine-complex decomposition method

Tingru Chen[1], Takuya Hasegawa[1], Sung Hun Cho[2], Tomoyo Goto[2], Tohru Sekino[2],
Masato Kakihana[2], Shu Yin[1, *]

[1]Institute of Multidisciplinary Research for Advanced Material (IMRAM), Tohoku University, Sendai, Miyagi, Japan 980-8577

[2]The Institute of Scientific and Industrial Research, Osaka University, 8-1, Mihogaoka, Ibaraki, Osaka 567-0047, Japan

* Corresponding author: Prof. Shu Yin, E-mail: yin.shu.b5@tohoku.ac.jp

Introduction

The complex cobalt oxide $YBaCo_4O_{7+\delta}$ has a unique ability to reversibly adsorb and desorb large amounts of oxygen ($\delta = 1.4$, OSC≈1225 μmol-O_2/g) in an exceptionally low-temperature range compared with traditional oxygen storage material CeO_2-ZrO_2 (OSC≈750 μmol-O_2/g) [1], which makes it a promising candidate for application in large oxygen storage capacity. According to the previous studies [2-6], $YBaCo_4O_{7+\delta}$ was prepared by sol-gel method or solid-state reaction at high-temperature calcination process (over 1050 °C) and exhibited high oxygen storage capacity. However, it is inevitable that the calcination process at such high-temperature conditions resulted in significant grain growth, formed large particles, and small specific surface area, which resulted in the poor kinetics of the oxygen intake/release process and low oxygen storage/release speed. In this case, this research focuses on the synthesis of $YBaCo_4O_7$ at low calcination temperature, improving the oxygen storage/release speed, and investigating the mechanism of rapid oxygen storage for the low-temperature sample.

Synthesis process

The detailed synthesis process is shown in scheme S1. For the 800 ℃ sample (named as YBCO-800), 0.004mol of Cobalt(II) nitrate, hexahydrate ($Co(NO_3)_2 \bullet 6H_2O$ 99.5%) and 0.001mol of Yttrium(III) nitrate, hexahydrate ($Y(NO_3)_3 \bullet 6H_2O$ 99.9%) and 0.001mol barium(II) nitrate ($Ba(NO_3)_2$ 99%) were dissolved in the 0.8mol/L glycine solution (30ml) and stirred at room temperature to obtain the homogeneous solution. Subsequently, 1.0 ml ethylene glycol (EG) was used as dispersant and stabilizer added into the solution to form a metal–glycine complex through a chelating process. The homogeneous solution was stirred at 200 °C for 1 h to form the red gel. This gel product was calcined at 450 °C for 3 h in an air atmosphere to obtain the precursors. The precursor was ground, then calcined at 800 °C in N_2 atmosphere for 12h. For the high temperature sample (950 ℃ sample, named as YBCO-950), the same raw materials were dissolved in the 0.2mol/L glycine solution (30ml) and obtained the precursors, finally calcined at 950 ^{o}C in the air for 12h with the heating rate of 5 °C/min and then natural cooling to room temperature.

Structural characterization

X-ray powder diffraction (XRD: D2 PHASER/BRUKER) with Cu-Kα radiation (λ = 0.15418 nm) was carried out to measure the phase composition and lattice parameter. Rietveld refinements of the measured XRD results were performed using the RIETAN-FP software package to confirm the exact crystal structure. For the high-temperature XRD (HT-XRD), approximately 50 mg sample was put into the heating device, which was combined with XRD equipment. The test process was carried out in a static air atmosphere in the temperature range 30−500 °C with a heating rate of 10 ℃/min. According to the TG curves, the sample has almost no weight increase in the low-temperature range, and we set to collect one XRD information of the test sample every 50 ℃ in the range of 30-180 ℃. Subsequently, one XRD data was recorded every 10 ℃ from 200 ℃ to 500 ℃ to observe the detailed structural change during the oxygen storage process. The particle sizes and morphologies of as-prepared samples were observed by scanning electron microscopy

(SEM, JEOL JSM-7800F) combined with energy-dispersive X-ray spectroscopy (EDS). Moreover, transmission electron microscopy (TEM, JEOL JEM-2100 microscopy) combined with the selected-area electron diffraction (SAED) patterns were performed to observe the detailed crystal structure. The specific surface area of as-prepared samples was evaluated by the Brunauer−Emmet−Teller (BET) formula using the adsorption isotherm obtained by the nitrogen adsorption method. To investigate the chemical states for each chemical species, the X-ray photoemission spectroscopy (XPS; PHI5600, ULVAC-PHI Inc.) using a monochromatized X-rays of AlKα (300 W). The Co K-edge X-ray Absorption fine structure (XAFS) spectra of the prepared and reference samples ($LiCoO_2$ for Co(III) and $2CoCO_3•3Co(OH)_2$ for Co(II)), which were prepared by mixing with the boron nitride powder. The beamline BL12C was used to collect the data at the Photon Factory (The High Energy Accelerator Research Organization, Japan (KEK) in transmittance modes).

Thermogravimetric measurement

A TG analyzer (TG8120/Rigaku) was utilized to evaluate the oxygen storage capacity. The *ca.* 20 mg powder sample was put into a Pt pan, and heated sample from 30 to 500 °C in the O_2 or air atmosphere with a flow rate of 100 mL/min gas. The heating/cooling rate was 1 °C/min. In order to evaluate the oxygen storage/release speed of these two samples, isothermal TG curves were recorded at different operating temperatures 350/360/370 °C associated with the nitrogen atmosphere and oxygen atmosphere switched each other. All the TG measurements are at ambient pressure.

Oxygen content analysis

The exact oxygen content was confirmed by iodometric titration from three parallel analyses. The sample (~20mg) and 1g KI were dissolved in 1M HCl solution to form iodine by reducing trivalent transition-metal cations. Then the 0.025 M $Na_2S_2O_3$ solution was used to evaluate the amount of iodine formed by the titration process. Starch as an indicator of the endpoint was added to the solution during the titration process. The endpoint was confirmed from the disappearance of blue color in the solution. The calculation of the Co^{3+} fraction was performed according to the equations:

$$Co^{3+}+I^{-}=Co^{2+}+0.5I_2 \qquad I_2+2S_2O_3^{2-}=2I^{-}+S_4O_6^{2-}$$

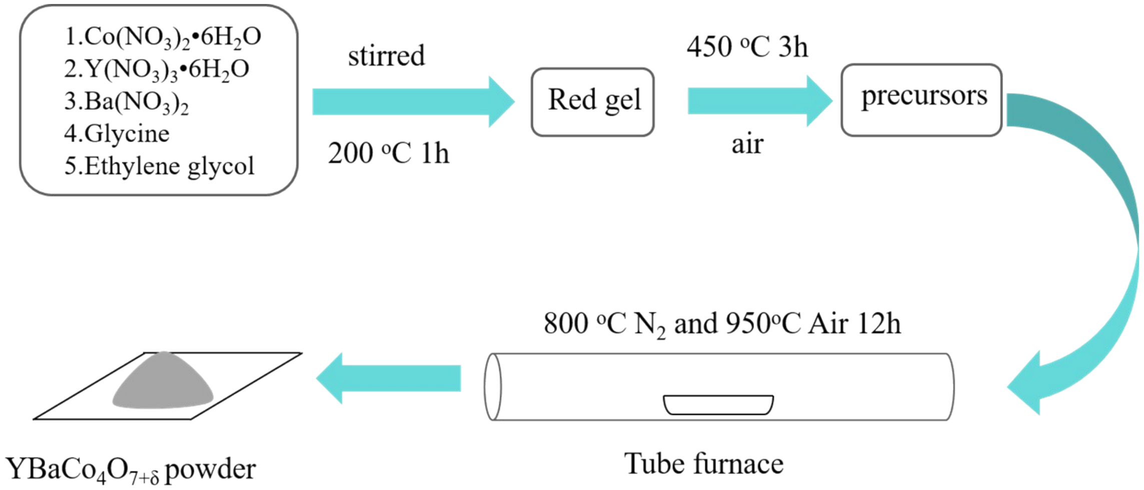

Scheme S1 Flow diagram for powder synthesis of $YBaCo_4O_7$ by the glycine-complex decomposition method

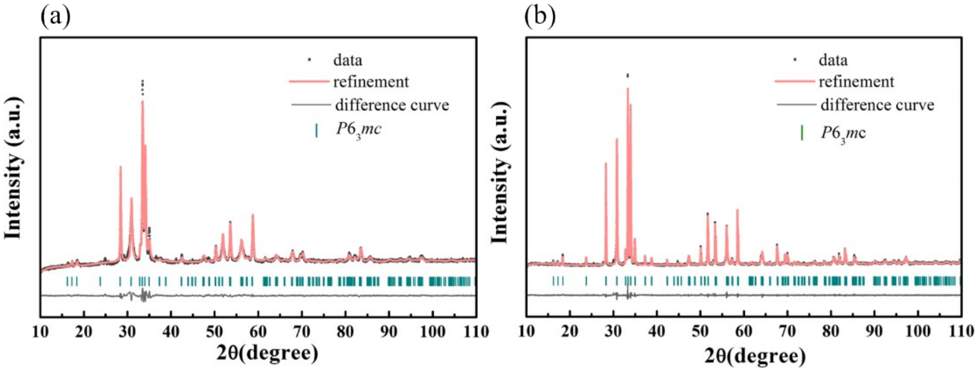

Fig. S1. XRD Rietveld results for $YBaCo_4O_{7+\delta}$. (a) 800 °C sample (N_2 atmosphere) (b) 950 °C sample (Air atmosphere)

Table S1. Lattice parameters of the as-prepared samples (S: goodness of fit).

Sample	a[Å]	c[Å]	V[Å^3]	Rwp[%]	Rp[%]	S
800°C	6.287(1)	10.261(2)	351.2(1)	2.6	1.6	2.1
950°C	6.296(3)	10.254(3)	352.1(2)	1.7	1.2	1.7

Table S2. Crystallographic parameters for $YBaCo_4O_{7+\delta}$ from the Rietveld refinement based on XRD data. (The atomic coordination z of O_2 site with 2a (Wyckoff symbol) was fixed to the same with CIF (ICSD #188853) as 0.74820 to set the origin)

Atmo	Site	x	y	z	Beq
800					
Y1	2b	0.3333	0.6667	0.192(5)	0.6(3)
Ba1	2b	0.3333	0.6667	0.578(5)	2.0(3)
Co1	2a	0	0	0.606(5)	1.1(3)
Co2	6c	0.8265(7)	0.17349	0.368(6)	1.3(3)
O1	6c	0.483(2)	0.51707	0.350(6)	2.0(7)
O2	2a	0	0	0.7482	0.3(2)
O3	6c	0.855(3)	0.14457	0.600(7)	5(1)
950					
Y1	2b	0.3333	0.6667	0.133(2)	1.5(1)
Ba1	2b	0.3333	0.6667	0.501(2)	0.82(8)
Co1	2a	0	0	0.555(3)	0.6(1)
Co2	6c	0.8301(3)	0.16993	0.312(2)	0.84(8)
O1	6c	0.482(1)	0.51849	0.268(2)	1.5(4)
O2	2a	0	0	0.7482	2.2(5)
O3	6c	0.843(1)	0.15685	0.515(3)	4.1(3)

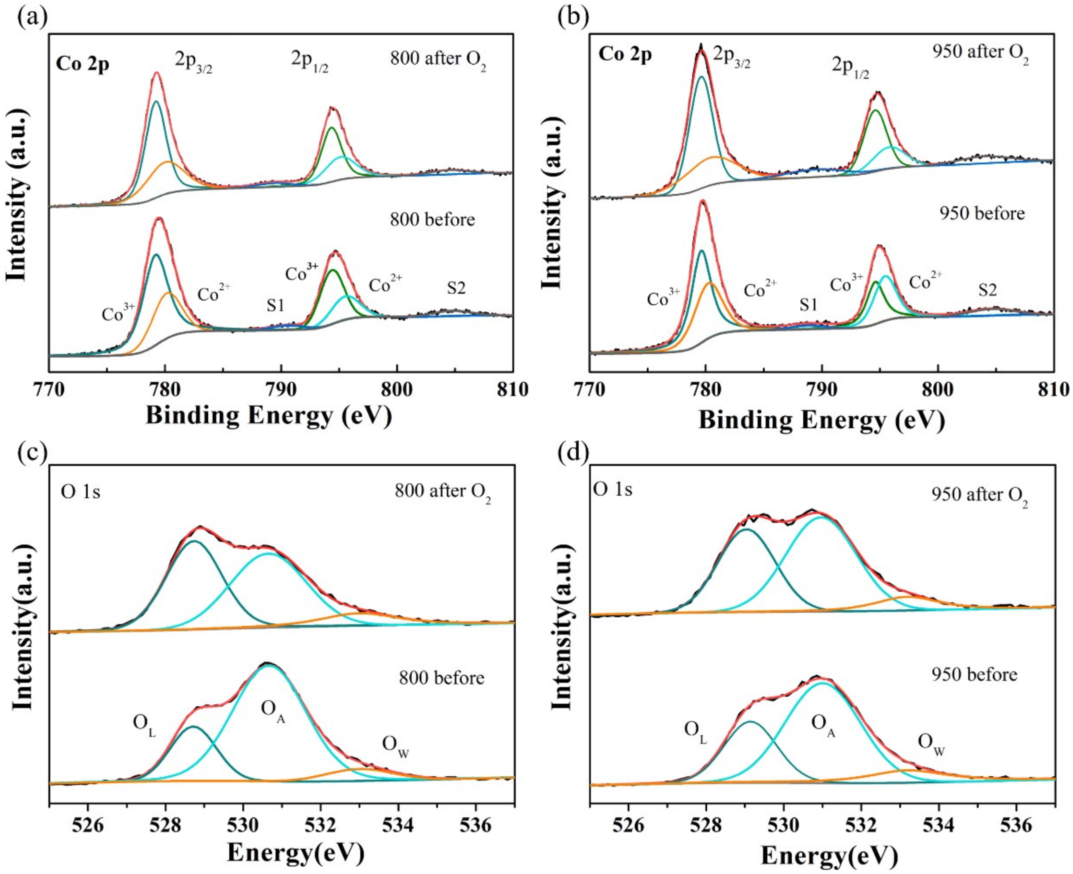

Fig. S2. XPS spectra of $YBaCo_4O_{7+\delta}$ before and after TG test for Co 2p regions (a-b) and O 1s regions (c-d), respectively.

Table S3 The ratio of Co^{3+}/Co^{2+} before and after TG measurement for $YBaCo_4O_7$ and iodometric titration results

sample	YBCO-800	YBCO-950
Before TG test Co^{3+}/Co^{2+}	1.45	1.36
After TG test Co^{3+}/Co^{2+}	2.05	2.11
Chemical formula (before TG)	$YBaCo_4O_{7.152}$	$YBaCo_4O_{7.024}$

Table S4. bonding energies and atomic percentages of 800 and 950 sample before and after TG measurement obtained from XPS analyses

Binding energies (eV)					
Before TG	Co $2p_{3/2}$		O 1s		
	Co^{3+}	Co^{2+}	O_L	O_A	O_W
YBCO-800	779.59	780.52	528.71(20.5%)	530.67(73.0%)	532.95
YBCO-950	779.53	780.38	529.14(30.5%)	531.00(51.4%)	533.14
After TG	Co $2p_{3/2}$		O 1s		
	Co^{3+}	Co^{2+}	O_L	O_A	O_W
YBCO-800	779.25	780.20	528.73(43.2%)	530.64(46.5%)	532.95
YBCO-950	779.45	780.20	529.05(40.5%)	530.97(49.0%)	533.11

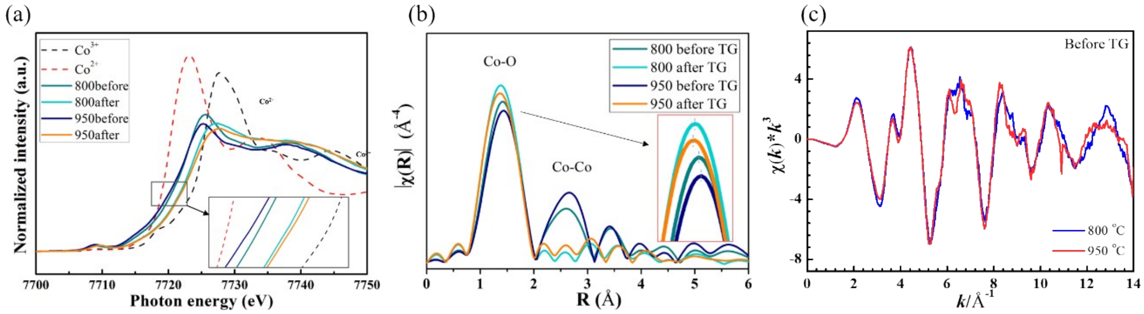

Fig. S3. XAFS results of $YBaCo_4O_{7+\delta}$. (a) Co K-edge XANES spectrum for two samples before TG test and after TG test at O_2 atmosphere (b) amplitude of Fourier transformed obtained from EXAFS oscillation before TG after TG. The weighted spectra were Fourier transformed in a k space of 3–10 $Å^{-1}$. (c) Co K-edge EXAFS oscillation of $YBaCo_4O_{7+\delta}$ before TG measurement.

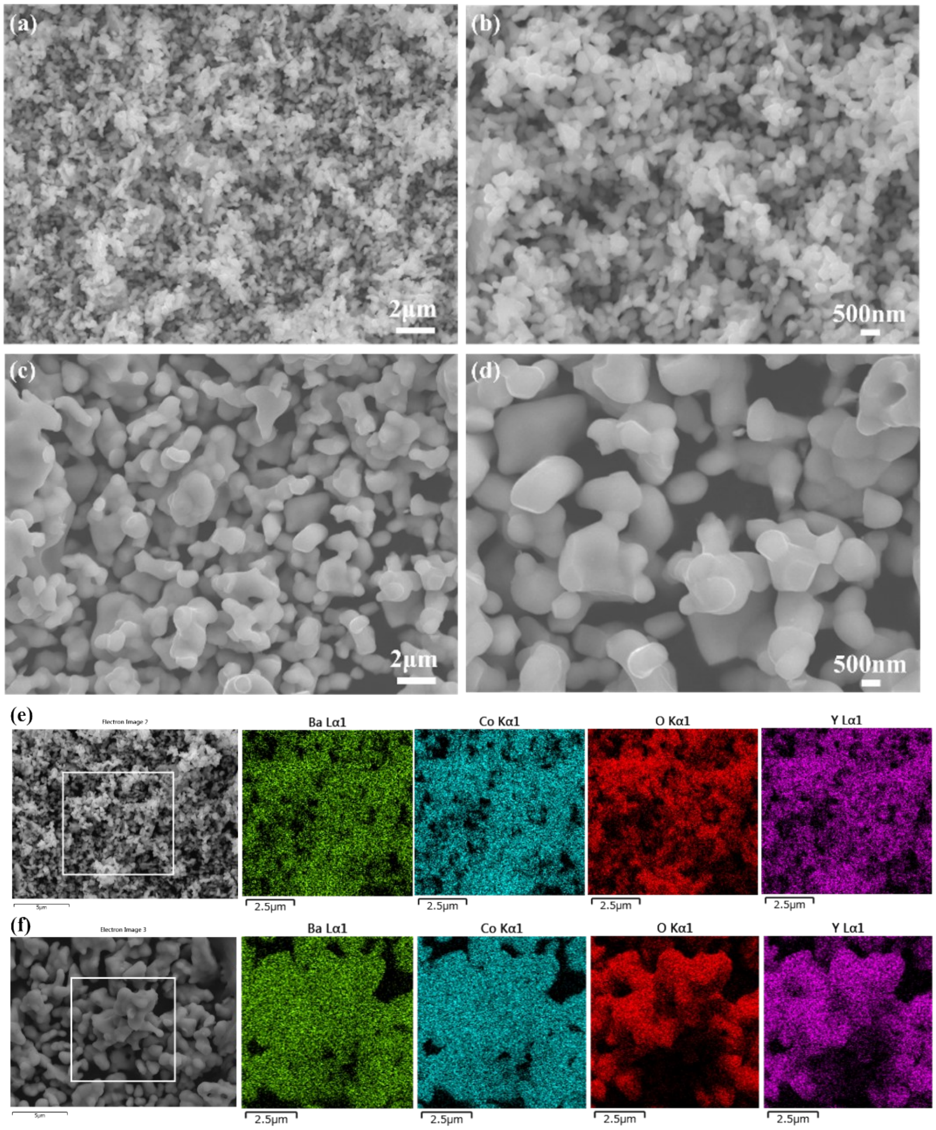

Fig. S4. SEM images of $YBaCo_4O_{7+\delta}$ synthesized by different temperature. (a-b) 800 °C sample (N_2 atmosphere), (c-d) 950 °C sample (Air atmosphere). EDS mapping of 800 ℃ sample (e) and 950 ℃ sample (f).

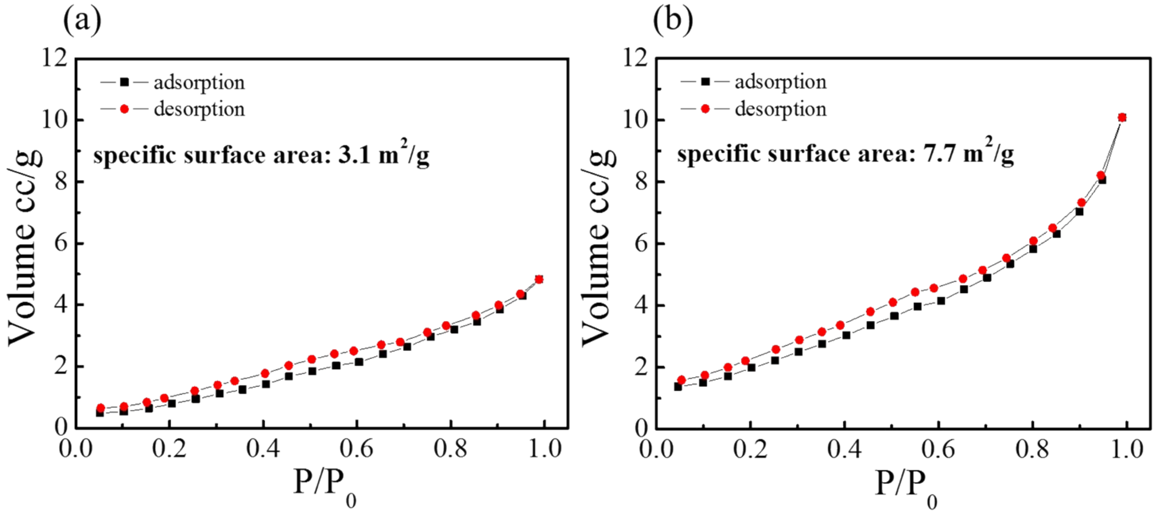

Fig. S5 Nitrogen sorption isotherms for BET surface area analysis for $YBaCo_4O_7$ obtained at different calcination temperature. (a) 950 ^oC sample (b) 800 ^oC sample

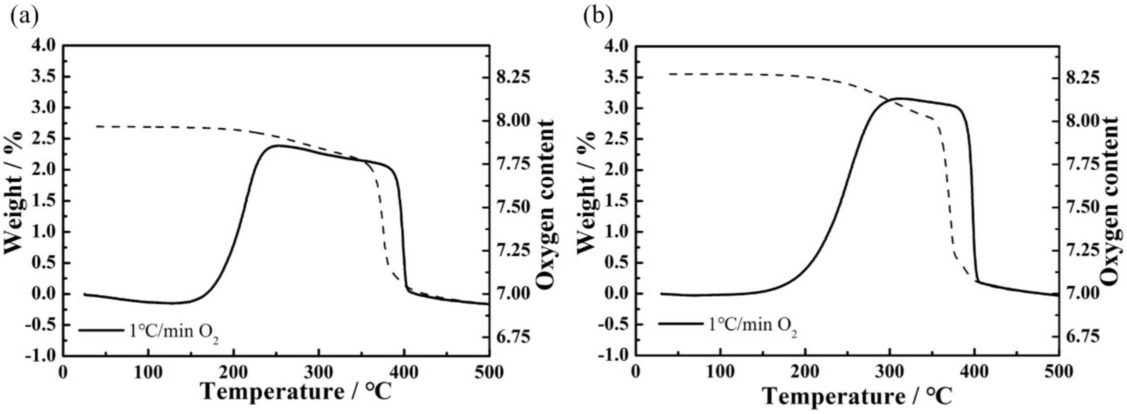

Fig. S6. TG curves of $YBaCo_4O_{7+\delta}$ in the oxygen atmosphere from 30 to 500 °C with heating/cooling rates of 1 °C/min. (a) 800 ^oC (N_2 atmosphere), (b) 950 ^oC (Air atmosphere). Heating curve: solid lines; cooling curve: dotted lines

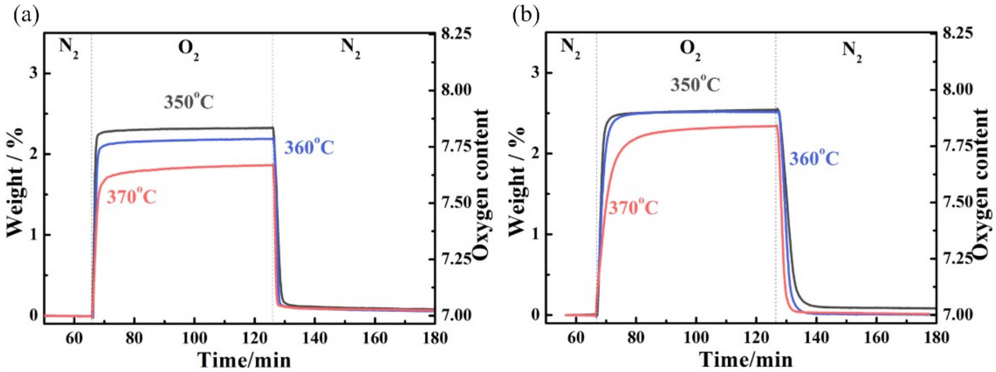

Fig. S7. Isothermal TG curves recorded in the nitrogen and oxygen atmosphere for $YBaCo_4O_{7+\delta}$ synthesized at different temperature. (a) 800 ^oC sample and (b) 950 ^oC sample.

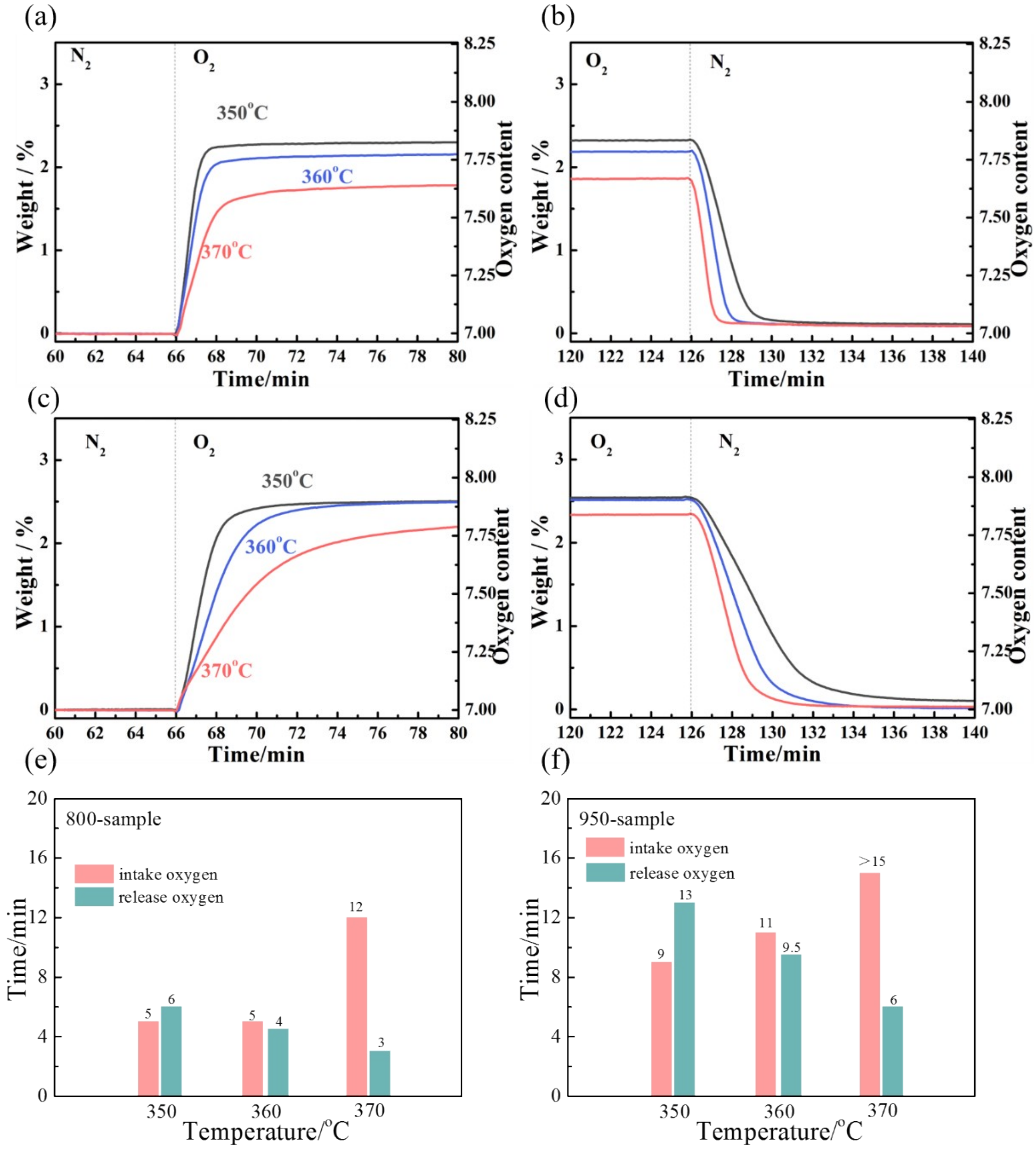

Fig. S8. Enlarged Isothermal TG curves recorded in the nitrogen and oxygen atmosphere $YBaCo_4O_{7+\delta}$ synthesized at different temperature. (a) 800 °C (N_2 atmosphere)-oxygen intake process (b) 800 °C (N_2 atmosphere)-oxygen release process (c) 950 °C (Air atmosphere)-oxygen intake process (d) 950 °C (Air atmosphere)-oxygen release process. Oxygen intake/release time of the $YBaCo_4O_{7+\delta}$ for 800 sample (e) and 950 sample (f).

Table S5 Oxygen storage capacity and oxygen intake/release time of $YBaCo_4O_{7+\delta}$ materials reported in previous research.

Samples	OSC(wt.%)	Intake/release time 350 ℃
$YBaCo_4O_{7+\delta}$ (This work)	2.33	5min/6min
$YBaCo_4O_{7+\delta}$ [7]	2.45	9min/＞20min
$YBaCo_4O_{7+\delta}$ [7]	2.66	16min/＞20min
$YBaCo_3AlO_{7+\delta}$[8]	1.00	＞1h
$YBaCo_4O_{7+\delta}$ [9]	3.32	＞1h
$YBaCo_{3.6}Al_{0.4}O_{7+\delta}$[4]	1.20	＞20min
$YBaCo_4O_{7+\delta}$ [10]	2.90	＞20min

To the best of our knowledge, the oxygen storage/release speed of the YBCO-800 sample synthesized by the glycine-complex decomposition method showed the highest intake/release speed among all the $YBaCo_4O_{7+\delta}$ materials according to the previous reports, as shown in Table S5. The intake and release of O_2 might be finished with 5/6 min at 350 ℃. Moreover, the time required for complete oxygen release was even reduced to 4 minutes at 360 ℃. These results further demonstrate that the glycine-complex decomposition method effectively reduces the calcination temperature and improves the oxygen storage/release speed.

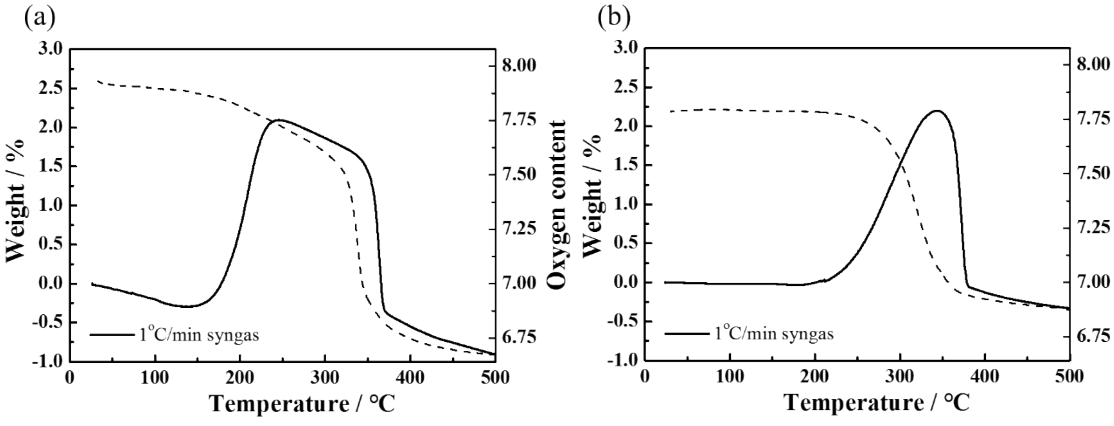

Fig. S9. TG curves of $YBaCo_4O_{7+\delta}$ in the simple air atmosphere (21% O_2 and 79% N_2) from 30 to 500 °C with heating/cooling rates of 1 °C/min. (a) 800 °C sample (b) 950 °C sample. Heating curve: solid lines; cooling curve: dotted lines

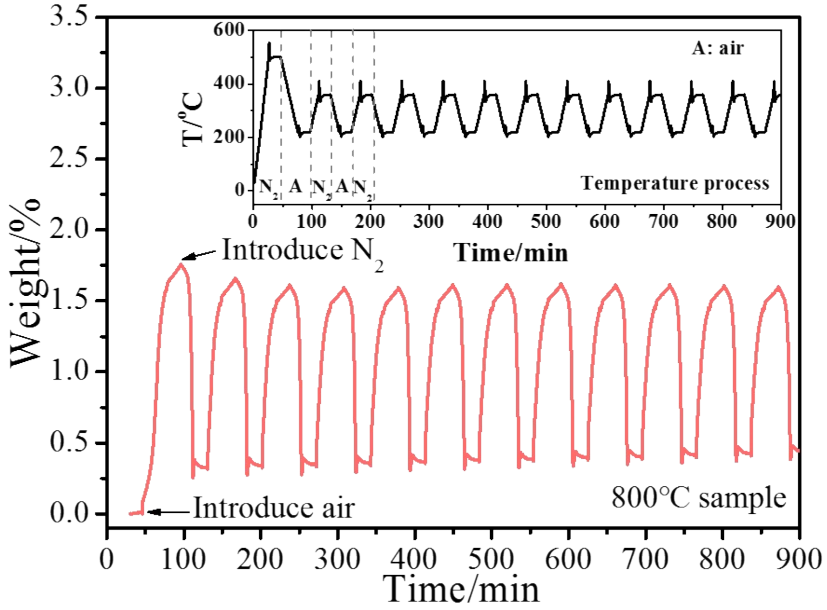

Fig. S10 Long cycle performance of 800°C sample measured by TSA processes during swing between 220 and 360 °C. N_2 is the reducing gas , air is the oxidizing gas. (insert picture: temperature process)

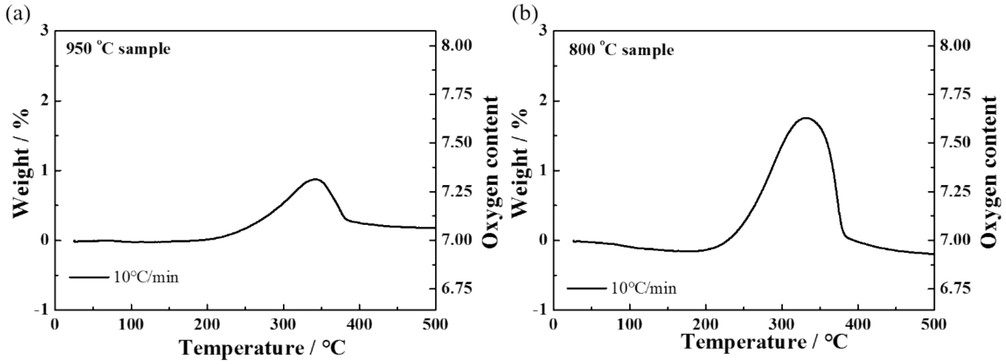

Fig. S11. TG curves of $YBaCo_4O_{7+\delta}$ in the air atmosphere from 30 to 500 °C with a heating rate of 10 °C/min. (a) 950 °C sample, (b) 800 °C sample.

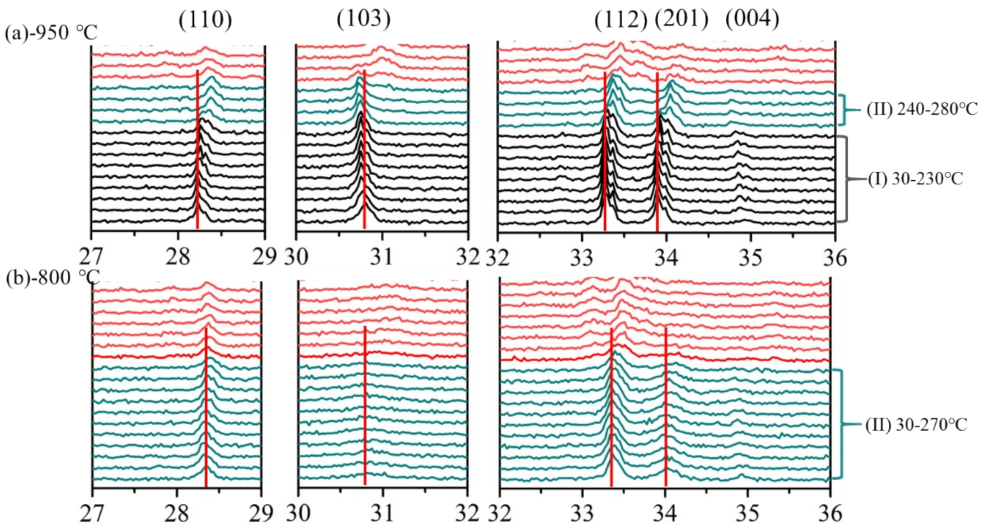

Fig. S12. Enlarged in-situ high-temperature XRD patterns of these two samples in the range of 30-280℃ for 950 ℃ sample, initial phase and intermediate phase (a) and in the range of 30-270℃ for 800℃ sample, intermediate phase (b).

Table S6 The main peak position of these two samples at room temperature and 240℃

Peaks	YBCO-950 (30℃)	YBCO-950 (240℃)	YBCO-800 (30℃)	YBCO-800 (240℃)
(110)	28.23°	28.38°	28.35°	28.35°
(103)	31.81°	30.73°	30.81°	30.81°
(112)	33.27°	33.36°	33.36°	33.36°
(201)	33.90°	34.04°	34.02°	34.03°

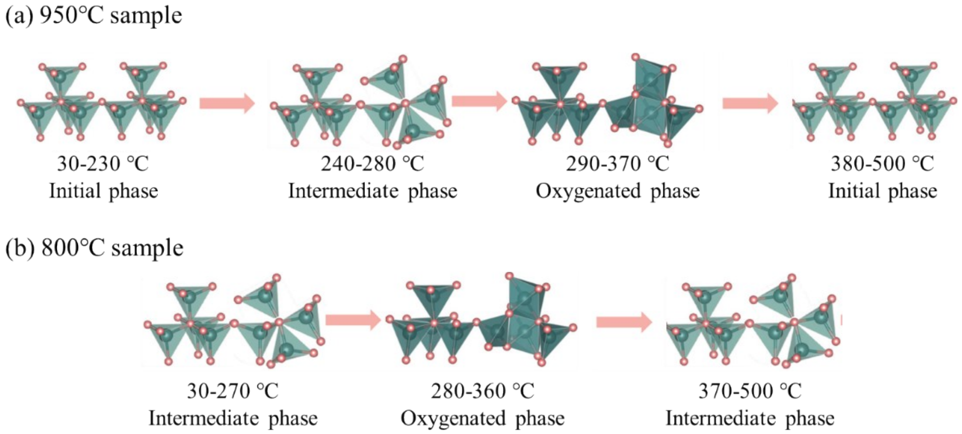

Fig. S13 Schematic diagram of structural changes during oxygen storage process

According to the data in the table, we can find that the peak position angles of the three main peaks (110), (112) and (201) of the 800 ℃ sample are higher than those of the 950℃ sample at room temperature, while the (103) peak represents the unique super-lattice structure of 800 °C sample based on our previous results. However, at high temperature 240 °C, three main peaks (110), (112) and (201) of 950 °C sample shift to a higher angle and their peak positions are almost the same as those of 800 °C sample, as shown in the Table. This result indicated that crystal phase of 800 °C is the same as the intermediate phase which formed during the heating process of 950 °C sample. This result can be illustrated with the following pictures (Fig. S13). In the initial heating process, there is no obvious peak shift for 950 °C sample. The peaks start to shift at 240 °C due to the heat treatment induced a cell expansion to adapt to the change from CoO_4 tetrahedron to CoO_6 octahedron during the oxygen storage process. In this case, intermediate phase formed at this temperature, as shown in Fig. S13(a). However, for the 800°C sample, we directly obtained the intermediate phase through low-temperature calcination of the precursor and this intermediate phase directly changed to oxygenated phase at high temperature.

Reference:

[1] O. Parkkima, H. Yamauchi and M. Karppinen, Chem. Mater., 2013, 25, 599-604.

[2] H. S. Hao, J. H. Cui, C. Q. Chen, L. J. Pan, J. Hu, X. Hu, Solid State Ionics 2006, 177, 631–637.

[3] M. Karppinen, H. Yamauchi, S. Otani, T. Fujita, T. Motohashi, Y.H. Huang, M. Valkeapaa, H. Fjellvag, Chem. Mater., 2006, 18, 490-494.

[4] T. Komiyama, T. Motohashi, Y. Masubuchi, S. Kikkawa, Mater. Res. Bull., 2010, 45, 1527-1532.

[5 S. Räsänen, T. Motohashi, H. Yamauchi,M. Karppinen, J. Solid. State. Chem., 2010, 183, 692-695.

[6] M. Xu, I. Ermanoski, E.B. Stechel, S. Deng, Chem. Eng. J., 2020, 389, 124026.

[7] Chen, T. R.; Asakura, Y.; Hasegawa, T.; Motohashi, T.; Yin, S. J. Mater. Sci. Technol. 2021, 68, 8−15.

[8] Valldor, M.; Hollmann, N.; Hemberger, J.; Mydosh, J. A. Phys. Rev. B 2008, 78, No. 024408.

[9] Hao, H. S.; Zhao, L. M.; Hu, J.; Hu, X.; Hou, H. W. J. Rare Earth. 2009, 27, 815−818.

[10] Karppinen, M.; Yamauchi, H.; Otani, S.; Fujita, T.; Motohashi, T.; Huang, Y. H.; Valkeapaa, M.; Fjellvag, H. Chem. Mater. 2006, 18, 490−494.